PAPER • OPEN ACCESS

Micromagnetic investigation of domain and domain wall evolution through the spin-reorientation transition of an epitaxial $NdCo_5$ film

To cite this article: Marietta Seifert *et al* 2017 *New J. Phys.* **19** 033002

New Journal of Physics
The open access journal at the forefront of physics

Deutsche Physikalische Gesellschaft DPG
IOP Institute of Physics

Published in partnership with: Deutsche Physikalische Gesellschaft and the Institute of Physics

OPEN ACCESS

RECEIVED
29 September 2016

REVISED
16 January 2017

ACCEPTED FOR PUBLICATION
16 February 2017

PUBLISHED
1 March 2017

PAPER

Micromagnetic investigation of domain and domain wall evolution through the spin-reorientation transition of an epitaxial $NdCo_5$ film

Marietta Seifert[1,3], Ludwig Schultz[1], Rudolf Schäfer[1], Sebastian Hankemeier[2], Robert Frömter[2], Hans Peter Oepen[2] and Volker Neu[1,3]

[1] IFW Dresden, Institute for Metallic Materials, PO Box 270116, D-01171 Dresden, Germany
[2] Universität Hamburg, Institut für Angewandte Physik, Jungiusstrasse 11, D-20355 Hamburg, Germany
[3] Authors to whom any correspondence should be addressed.

E-mail: marietta.seifert@ifw-dresden.de (M.S.) **and** v.neu@ifw-dresden.de (V.N.)

Keywords: $NdCo_5$, spin reorientation transition, micromagnetic simulation, scanning electron microscope with polarisation analysis, thin film, pinning, domain pattern

Abstract

The domain pattern and the domain wall microstructure throughout the spin-reorientation transition of an epitaxial $NdCo_5$ thin film are investigated by micromagnetic simulations. The temperature-dependent anisotropy constants K_1 and K_2, which define the anisotropy energy term in the model, are chosen to reflect the easy axis—easy cone—easy plane spin-reorientation transition observed in epitaxial $NdCo_5$ thin films. Starting at the high-temperature easy *c*-axis regime, the anisotropy constants are changed systematically corresponding to a lowering of the temperature of the system. The character of the domain walls and their profiles are analysed. The calculated domain configurations are compared to the experimentally observed temperature-dependent domain structure of an in-plane textured $NdCo_5$ thin film.

1. Introduction

The intermetallic $NdCo_5$ phase, which belongs to the group of the rare-earth-transition metal compounds, is interesting not only from a fundamental point of view due to its spin-reorientation transition (SRT) from a magnetic easy *c*-axis at high temperatures via a magnetic easy cone to a magnetic easy plane at low temperature, but also for possible applications, which exploit the huge change in magnetocrystalline anisotropy that occurs at temperatures between 310 and 255 K, i.e. close to room temperature. One example is the possible application in magnetic refrigeration owing to a giant rotating magnetocaloric effect [1]; another is the transfer of anisotropy to a soft magnetic layer in a $NdCo_5$/Fe bilayer system [2]. In the past, this material has been prepared and investigated mainly as bulk samples [3–9]. Only recently we achieved epitaxial growth with either in-plane [10] or out-of-plane [11] texture, which enables to study the spin-reorientation transition also in thin films.

For the most part, investigations of the SRT deal with global magnetisation measurements. To analyze the domain structure at the surface of in-plane textured $NdCo_5$ thin films with sufficient spatial resolution, we recently used scanning electron microscopy with polarisation analysis (SEMPA) [12]. This method [13] allows imaging the local in-plane magnetisation direction. As also cooling is possible with this particular device, the change of the magnetisation pattern throughout the full spin-reorientation-transition can be imaged. As a main result of this investigation it was shown, that—using a sample in the as-prepared state—in the easy *c*-axis regime above 318 K there is a two-domain state with an orientation of the magnetisation along the magnetic easy *c*-axis. When the sample is cooled down, a four-domain state evolves, where the four directions of magnetisation correspond to the four easy magnetisation directions that result from the intersection of the magnetic easy cone (magnetocrystalline anisotropy) and the magnetic easy plane parallel to the film plane which is determined by the shape anisotropy. Figure 1 shows an exemplary image of the $NdCo_5$ film at a temperature of 300 K. Clearly visible is the complicated domain structure with an orientation of magnetisation in four directions, which correspond to the four directions of the magnetic easy cone. Furthermore, the domain walls occupy

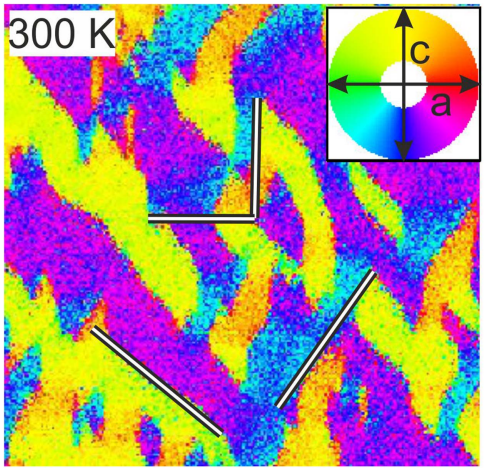

Figure 1. SEMPA image of a $NdCo_5$ thin film at 300 K. At this temperature, the magnetic easy cone has slightly opened ($\approx 23^\circ$). The black/white lines indicate the three different orientations of domain walls: parallel to the *c*- and *a*-axis and 45° in between.

characteristic angles with respect to the crystallographic orientation, namely parallel to the *c*- and *a*-axis and at an angle of 45°. Finally, at temperatures below 252 K there is again a two domain state now with the magnetisation rotated by 90° and oriented parallel to the easy *a*-axis.

Reference [12] summarises an interpretation of the magnetisation processes which take place during the heating or cooling procedure via the different regimes of magnetocrystalline anisotropy.

However, there remain open questions concerning the character of the domain walls, which can be determined from SEMPA measurements only for a few special configurations. The character of the domain walls is still unknown for the various regimes of magnetocrystalline anisotropy. The theory of 180° domain walls for the case of an easy-axis magnetisation is well established [14], but there are only some preliminary theoretical considerations for 180° walls in bulk materials with easy-cone anisotropy [15].

For a deeper understanding of the magnetisation processes in epitaxial $NdCo_5$ thin films, micromagnetic simulations are performed to analyze the domains and the domain wall structure in all three regimes of magnetocrystalline anisotropy, namely easy-axis, easy-cone and easy-plane anisotropy.

It is known, that rare-earth–Co thin films contain pinning centres produced e.g. by grain boundaries, stacking faults within the unit cell of the hexagonal crystal, and local changes of the composition [16]. For $NdCo_5$ thin films, a pinning-dominated coercivity mechanism was demonstrated [10]. The temperature-dependent SEMPA measurements showed that the domain configuration remained nearly the same after several heating and cooling cycles. This behaviour was also attributed to a dense network of pinning centres, which are present in these thin film samples [12]. Therefore, one focus of the investigations will be on the effect of various types of pinning centres on the domain behaviour.

The results of the simulations will then be compared with experimental data obtained from SEMPA measurements.

2. Computer experiments

The calculations were performed with the software `MicroMagus` [17], a programme that allows the simulation of equilibrium magnetisation structures. These are found by minimising the magnetic free energy consisting of the magnetocrystalline anisotropy energy, exchange stiffness energy, stray field energy and the Zeeman energy in an external field. Since the aim was to analyze the equilibrium state without external fields, the latter energy was always zero.

The used geometry and the discretization are sketched in figure 2. There are 500 cells of 1 nm each in *x*- and *z*-direction (film plane) and seven layers with a thickness of 3 nm each in *y*-direction, which is perpendicular to the film plane. The *c*-axis of the material is oriented parallel to the *z*-axis. In the physical experiment, the high quality of epitaxial growth guarantees a close to uniform orientation of the *a*- and *c*-axes throughout the film. In the following sections, the positions of domain walls, pinning centres et cetera are denoted only by the number of the respective cells without indication of the unit 'nm'. The chosen discretization fulfills the condition that the size of the cells has to be in the range of the exchange length of the material (at 400 K: $\sqrt{A/K_1} = 2.9$ nm, $\sqrt{A/K_d} = 4.5$ nm with A being the exchange constant, K_1 the magnetocrystalline anisotropy constant of first order and $K_d = 0.53$ MJ m^{-3} the shape anisotropy constant). Since the results of the simulations are to be

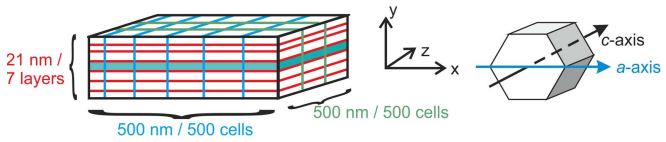

Figure 2. Discretization used for the simulations together with a sketch of the orientation of the $NdCo_5$ unit cell. In the following, the simulation results of the 4th layer, which is marked with colour, are presented and discussed.

Table 1. Temperatures and anisotropy constants used for the simulations [12].

Temperature	(K)	400	300	285	261	200
K_1	(MJ m^{-3})	1.20	−0.15	−0.72	−1.58	−4.80
K_2	(MJ m^{-3})	0.26	0.70	0.77	0.88	1.15
θ_{SR}	(°)	0	19	43	71	90

compared with measurements of an extended thin film, the boundary condition in the x–z-plane was set periodic.

The calculations were performed for selected 'temperatures', i.e. the respective magnetocrystalline anisotropy constants of first and second order, which were derived from global vibrating sample magnetometry measurements and local SEMPA measurements [12], were used as parameters in the programme. The temperatures, the values of K_1 and K_2 and the resulting spin-reorientation angle θ_{SR} are summarised in table 1. The angle θ_{SR} describes the easy direction of magnetisation with respect to the c-axis. It is 0° in the easy-axis regime and 90° in the easy-plane case. The exchange stiffness constant A of $NdCo_5$ at room temperature is 1.05×10^{-11} J m^{-1} [18], which is assumed to be constant at all temperatures. It is important to remark that no thermal activations are considered, so that actually the calculations are performed at a temperature of 0 K.

3. Results and discussion

This section will treat two aspects. In section 3.1 a completely homogeneous sample will be considered, meaning that all cells of the geometry have the same material properties. This will be named 'undisturbed situation'. In section 3.2 inhomogeneities are added to investigate the influence of pinning centres on the magnetisation configuration. This is done by changing an intrinsic property, like the value of the exchange stiffness, the saturation magnetisation or the magnetocrystalline anisotropy in some cells ('disturbed situation').

3.1. Undisturbed situation

The calculations were started with the simplest case, which is the easy-axis (uniaxial) scenario. As an example, the equilibrium magnetisation configuration at 400 K is calculated. The anisotropy constants $K_1 = 1.20$ MJ m^{-3} and $K_2 = 0.26$ MJ m^{-3} were used (see table 1).

As initial configuration, the magnetisation was set to lie parallel to the positive z-direction for all cells with $0 \leqslant x \leqslant 247$ and to the negative z-direction for $253 \leqslant x \leqslant 500$. In-between ($248 \leqslant x \leqslant 252$) the y-component of M/M_S was chosen as +1. Without this presetting, the simulation results in a segmented Bloch wall. Since the aim was to perform simulations for various conditions (with or without addition of pinning centres) and to compare the results, a defined initial configuration was necessary. This was achieved by presetting the m_y component in the region of the domain wall, as it is described above.

The simulation results in a Bloch wall between the two domains, as can be seen in figure 3(a). A comparison of this wall with the analytical solution will be shown in section 3.2.1. The arrows in figure 3 represent the projection of magnetisation in the x–z-plane and the underlying colour code indicates the y-component. The character of the wall at 400 K (figure 3(a)) becomes obvious from the y-part that reaches the value of 1 at the interface between the two domains. In all cases discussed, the magnetic structure is essentially independent of y and therefore only one layer is sufficient to illustrate the behaviour. Thus, the magnetisation of the 4th layer, which is the layer in the centre of the geometry, is shown.

Besides the easy-axis scenario at 400 K, we want to focus on three interesting cases: the transition between easy axis and easy cone where K_1 becomes zero, an example of the easy-cone regime for the cone opening angle of 43°, and an example for the easy-plane state.

The results of the calculation for 400 K are used in the next step as initial magnetisation configuration for the following simulation with the anisotropy constants valid at the next lower temperature and so on. This

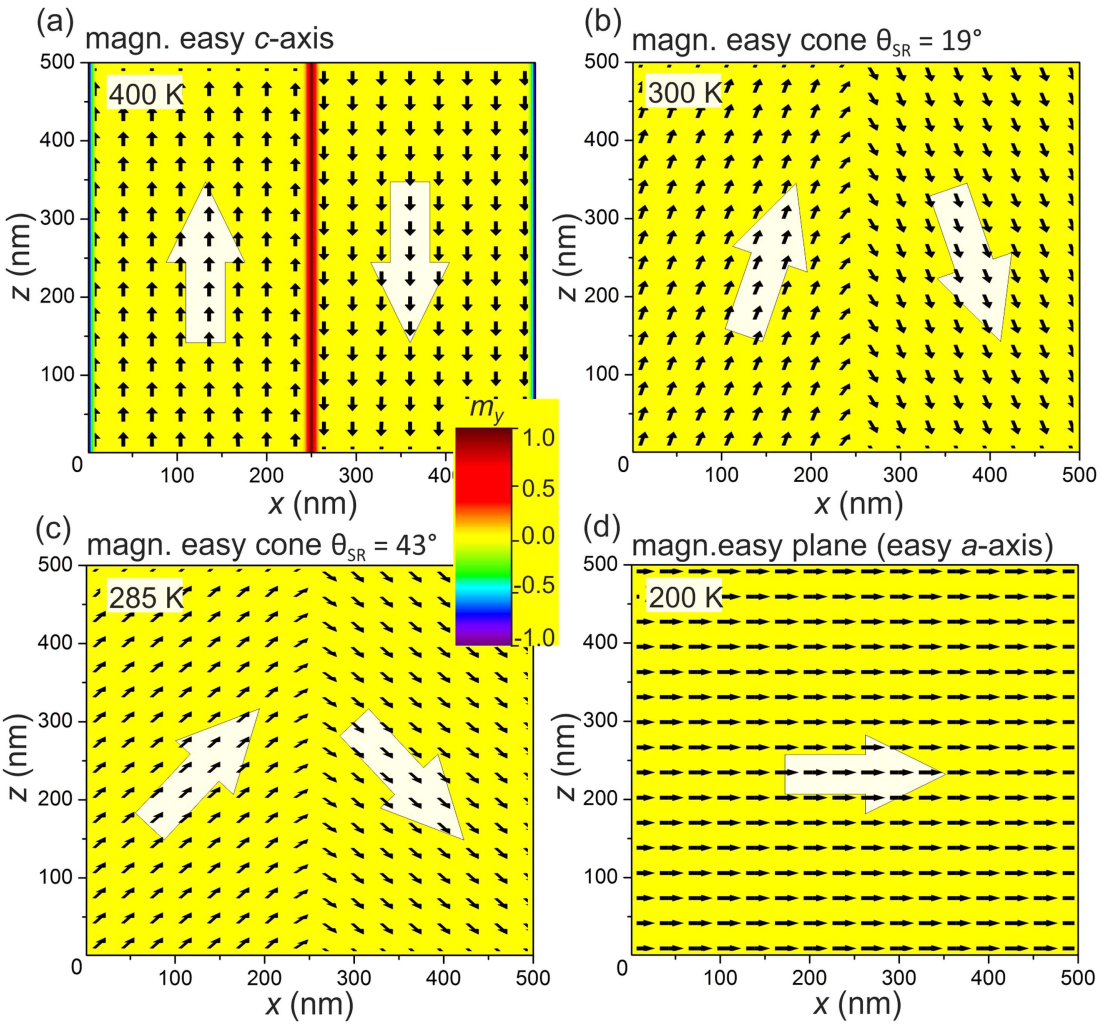

Figure 3. Magnetisation projected on the x–z-plane (arrows) with underlying colour-code representing the y-component for the undisturbed configuration at (a) 400 K, (b) 300 K, (c) 285 K, and (d) 200 K. The light coloured arrows indicate the averaged direction of magnetisation within the domains.

procedure corresponds to a stepwise 'cooling' of the sample and allows to follow the changes of domain walls and domain structure through the SRT.

In the second step, the configuration at 300 K was simulated. At this temperature the magnetic easy cone has slightly opened. The calculated domain pattern is again a two-domain state but now with a tilted orientation of magnetisation with respect to the c-axis. In both domains, the magnetic moments are tilted in the same (positive) x-direction (figure 3(b)). This way, magnetic charges are avoided at the boundaries between the two domains. Also, no magnetic charges are accumulated at the borders of the geometry, since the sample is infinitely extended (periodic boundary conditions). The angle of the spins with respect to the c-axis (z-direction) corresponds to the opening angle of the magnetic cone of 19°. In contrast to the situation at 400 K, the two domains are not separated by a Bloch wall, but by a Néel wall. All magnetic moments lie within the film plane. Lowering the temperature further (285 K) leads to a further increase of the x-component in accord with a larger cone opening angle and finally at 200 K the sample is fully magnetised in the positive x-direction (figures 3(c) and (d)). Except for the Bloch wall which is introduced in the 400 K scenario in all cases there is no out-of-plane component of the magnetisation.

These calculated results are not in agreement with the SEMPA-measurements, where all four possible directions of magnetisation are present in the easy cone regime and a two-domain instead of the saturated state is observed for the easy-plane case. This discrepancy can be understood as result of the impurities and pinning centres which will have an influence on the domain pattern. This issue will be discussed in the next section.

3.2. Disturbed situation—addition of pinning centres

This section will elucidate the effect of pinning centres on the magnetic configuration. For this purpose, three kinds of pinning centres are examined. In the first case the pinning centre is formed by a few cells with reduced

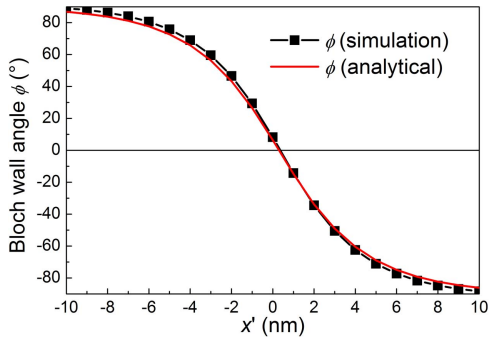

Figure 4. Bloch wall angle derived from simulation (black squares) and analytical solution (red, [14]). The x-axis is shifted so that the centre of the domain wall is located at $x' = 0$ nm.

exchange stiffness constant $A' = 1/2A$. In the second case, in some cells the saturation magnetisation is set to zero, which corresponds to a non-magnetic hole. Finally, the influence of pinning centres with reduced magnetocrystalline anisotropy constants is analyzed. The position of the pinning centre is described by the $(x|z)$ coordinates, which are the same in all seven layers.

3.2.1. Pinning centre with $A' = 1/2A$

As mentioned above, pinning centres can arise from stacking faults or local changes of composition. These effects influence the local anisotropy constant K but also the exchange stiffness constant A, so that as a first assumption for the simulations, regions of reduced exchange stiffness will be considered as pinning centres. Therefore the exchange constant A (1.05×10^{-11} J m^{-1}) has been chosen to be decreased to $1/2A$ in the rectangular areas $(x|z)$ of $(247|1) - (253|3)$ and $(247|498) - (253|500)$. Due to the periodic boundary conditions, these two centres form together one larger pinning centre.

400 K*:* the simulation again started with the anisotropy constants corresponding to a $NdCo_5$ thin film at 400 K. Using the same initial magnetisation configuration as in section 3.1 likewise results in an unsegmented Bloch wall, this time located between the two pinning centres. The Bloch wall character is again obvious from the out-of-plane component M_y/M_S. For analysing the domain wall the tilting angle ϕ, which is the angle between the direction of magnetisation and the film normal, is calculated. It is plotted in figure 4 together with the curve calculated from analytical theory [14]:

$$\tan\phi = \sqrt{1+\kappa}\,\sinh\left[x/\sqrt{A/K_1}\right]. \tag{1}$$

In this equation, κ is the ratio of the anisotropy constants: $\kappa = K_2/K_1$ and A the exchange constant of 1.05×10^{-11} J m^{-1}. Interestingly, the simulated and calculated curves are in good agreement which cannot be taken for granted since the theory holds for an infinitely extended domain wall, while the present micromagnetic calculation considers a film of only 21 nm thickness. The broad correspondence validates our numerical approach, including discretization intervals and geometry.

300 K*:* taking the results of 400 K as a starting point for the simulation at 300 K, which is very close to the transition from easy axis to easy cone, leads to a different result than in the case without pinning centres. Now a four-domain state evolves (figure 5). There are two Néel-type domain walls—one parallel to the crystallographic a-axis and another parallel to the c-axis. The magnetisation within the domains is oriented in-plane, since the possible directions of magnetisation on the surface of the magnetic easy cone are reduced to those four in-plane orientations that result from the intersection of the magnetic easy cone (magnetocrystalline anisotropy) with the magnetic easy plane determined by the shape anisotropy. An out-of-plane orientation within the domains is disadvantageous due to stray-field energy. Only at the intersections of the domain walls there is an out-of-plane component of magnetisation. At these points, either circular or cross Bloch lines are formed, which are marked in figure 5.

The correspondence between the easy magnetic direction and the orientation of magnetisation becomes obvious by plotting the orientation of the magnetic moments with respect to the c- and a-axes along the line profiles indicated in figure 5. The result is presented in figure 6. (For the definition of the angles ψ_1 and ψ_2 see figure 5.) According to this definition, ψ_1 varies in the range $-\theta_{SR} < \psi_1 < \theta_{SR}$ and for ψ_2 the relation $-90^\circ + \theta_{SR} < \psi_2 < 90^\circ - \theta_{SR}$ holds. For these graphs, the x- or z-axis is shifted such that the centre of the domain wall lies at $x' = 0$ nm or $z' = 0$ nm, respectively. The graphs show that on both sides of the domain wall, i.e. within the domains, the magnetic moments point parallel to the orientation determined by the in-plane opening angle of the cone. At 300 K, the domain wall parallel to the c-axis, where an angular interval of 142° has to be overcome, is much sharper than the wall parallel to the a-axis, which has to overcome 38°.

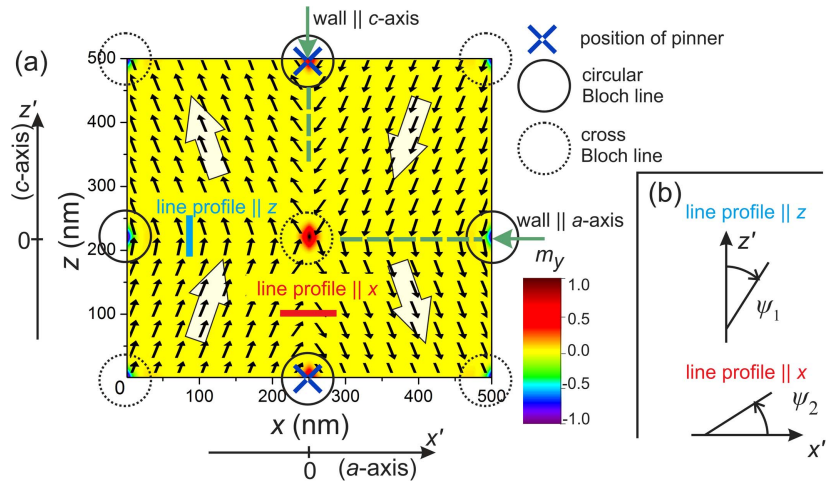

Figure 5. Magnetisation projected on the x–z-plane (arrows) with underlying colour-code representing the y-component for the situation at 300 K with exchange pinning centres. The light coloured arrows indicate the averaged direction of magnetisation within the domains. The circular and cross Bloch lines are marked by circles. On the right hand side, the definition of the angles ψ_1 and ψ_2 is sketched.

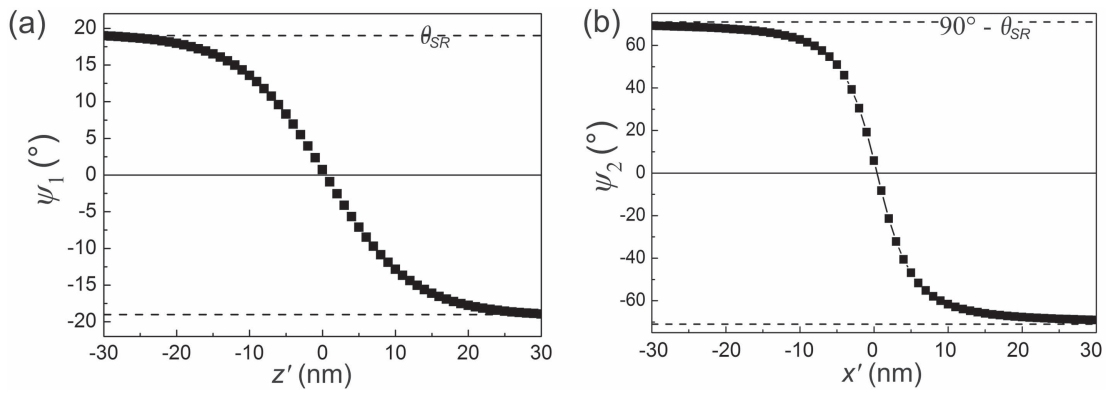

Figure 6. Orientation of the magnetic moments along the cross section of the domain wall parallel (a) to the a-axis and (b) to the c-axis at 300 K. For the definition of ψ_1 and ψ_2 see figure 5.

To analyze in detail the effect of reduced exchange pinning centres on the domain wall and to determine the origin of the formation of the four-domain state in the case of a disturbed situation, a further calculation is performed: a large region of 50 × 50 cells of reduced A is set in the centre of the calculated array. Due to the large size, the influence on the domain wall should be visible more clearly than for the small pinning centres considered before. The calculations are performed for 400 K and subsequently for 300 K.

Figure 7 shows a zoom-in of the x-, y- and z-component of the magnetisation calculated for the large pinning centre at 400 K. The dimension of the pinning centre is marked by the black square. The colour code represents the scale from plus to minus 1 for the y- and z-component of magnetisation. For m_x the scale has been expanded from $+0.04$ to -0.04. It can be clearly seen that in the region of reduced exchange stiffness the Bloch wall width δ_w is smaller as expected from $\delta_w = \sqrt{A/K}$.

A comparison of the three magnetisation components across the wall inside and outside the pinning centre is presented in figure 8(a), which manifests the smaller wall width. In addition, the simulated and analytical Bloch wall angle is sketched in figure 8(b), again confirming a good correspondence between both results.

In the zoomend-in image in figure 9(a) the x-component clearly shows a non-zero part at the intersection of the domain wall and the pinning centre. Already at 400 K this indicates a very weak but non-negligible rotation of the spins around the pinning centre, which is indicated by the black arrows in figure 9(a). This x-component is caused by magnetic charges which accumulate at the transition between the thinner and thicker domain wall and create magnetic stray fields as it is sketched in figure 9(c). Consequently, when the easy cone opens by reducing the temperature, the spins will follow this predefined chirality and a circular Bloch line will develop, as can be seen in figures 9(b) and (d).

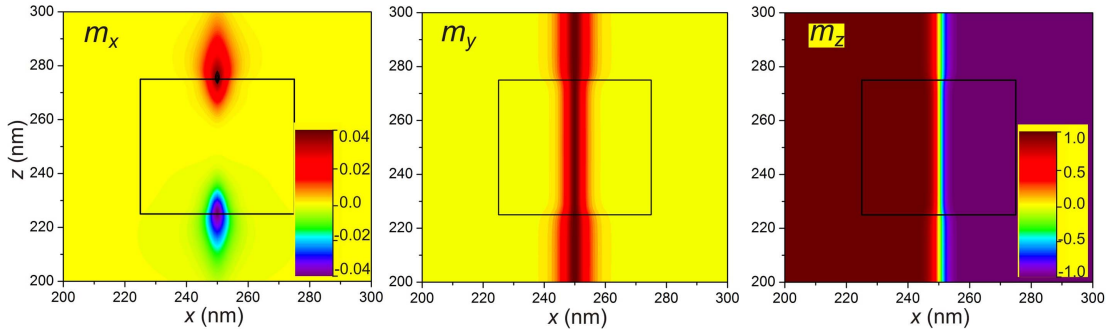

Figure 7. Zoomed-in *x*-, *y*- and *z*-component of the magnetisation calculated for the 50 × 50 cells large region of reduced exchange constant (indicated by the quadradic frame) at 400 K. The scale for the *x*-component has been expanded from +0.04 to −0.04.

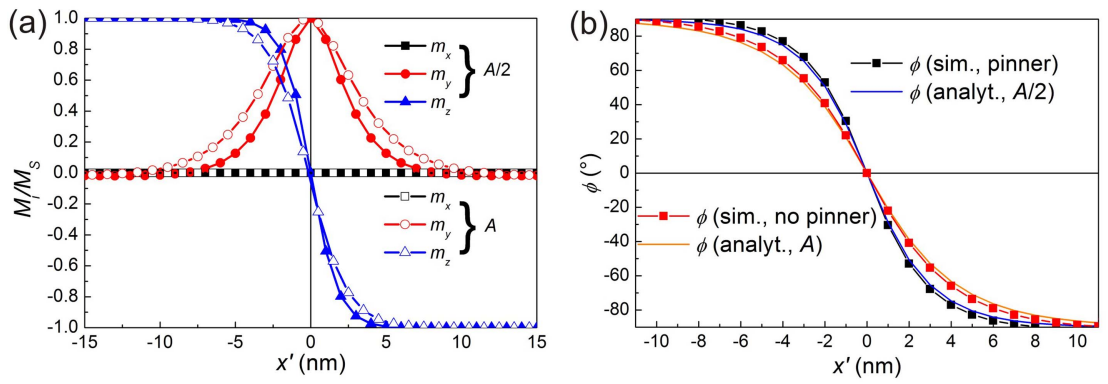

Figure 8. (a) Cross section of *x*-, *y*- and *z*-components of magnetisation through the Bloch wall in a region of reduced *A* (full symbols) and regular *A* (open symbols) and (b) simulated and analytical [14] Bloch wall angle ϕ.

285 K: proceeding with the results from 300 K to the next temperature of 285 K in the original model with small pinning sites, where the cone opening angle is 43°, the four-domain configuration is kept, but the character of the domain walls partly changes. While the wall parallel to the *c*-axis maintains its Néel character, the wall parallel to the *a*-axis now consists of alternating Bloch segments (figure 10(a)).

The difference in the walls parallel to the *a*- and *c*-axis can be explained by the difference of the wall orientation with respect to the easy cone. Proceeding from domain *I* to domain *II* in figure 10(a) the direction of magnetisation changes from the right-hand side to the left-hand side of the upper magnetic easy cone (see figure 10(b)). To realise this transition, the magnetisation can follow the surface of the magnetic easy cone, resulting in an out-of-plane component of the domain wall oriented parallel to the *a*-axis. In contrast, going from domain *I* to domain *III*, i.e. crossing a domain wall parallel to the *c*-axis, the direction of magnetisation changes from the right-hand side of the upper cone to the right-hand side of the lower cone (figure 10(c)). Here, the magnetisation cannot stay on the surface of the magnetic easy double cone. Therefore in the transition region it will chose the path of minimum out-of-plane component to save shape anisotropy energy and consequently a Néel wall is formed. Note that the influence of the shape anisotropy is also visible in a flattened out-of-plane component of the magnetic easy cone in the domain wall parallel to the *a*-axis (not shown). The magnetisation reaches an out-of-plane angle of 31°, which is less than θ_{SR} (43°) of the magnetic easy cone at this temperature. The maximum and minimum values of the *y*-component, which are ±0.51, are marked on the colour bar.

In the Bloch-type domain wall parallel to the *a*-axis, the energy is degenerated with respect to the out-of-plane polarity of the wall (m_y), resulting in a segmentation which leads to an additional decrease in stray-field energy along the wall length.

The orientation of the magnetic moments across both domain walls is shown in figure 11. It can be seen that within the domains the direction of magnetisation is determined by the spin-reorientation angle θ_{SR} of 43°.

200 K: a further cooling of the sample down to the easy-plane regime consequently leads again to a two-domain state. As expected, the two domains are magnetised in-plane parallel to the in-plane *a*-axis, which is now a magnetic easy axis (figure 12(a)). An out-of-plane orientation within the magnetic easy plane is less favourable due to the shape anisotropy. The two domains are separated by a Bloch wall, which is segmented equivalent to the situation at 285 K. A Bloch wall is energetically favoured because the magnetisation can rotate within the

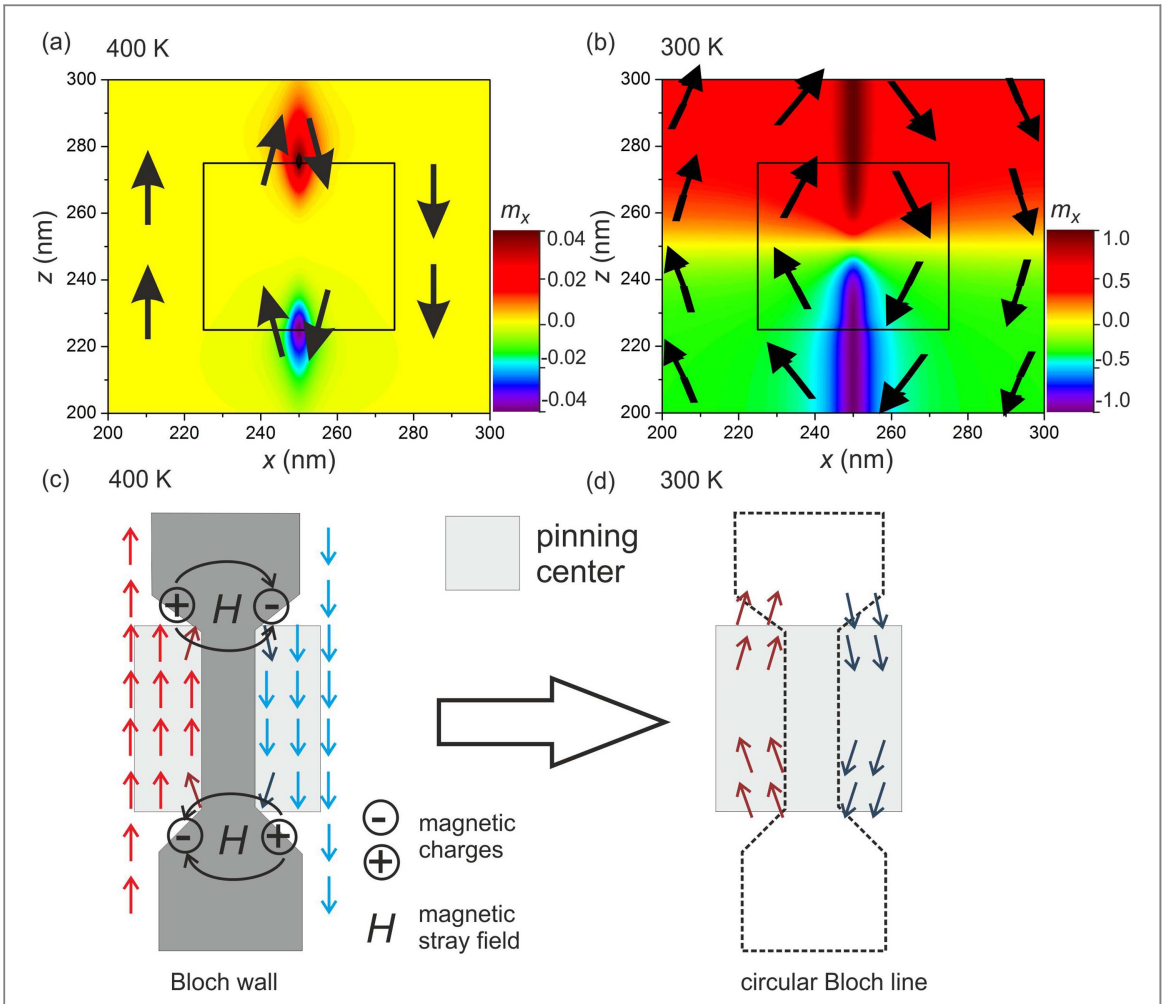

Figure 9. (a) Domain pattern at 400 K. (b) Domain pattern at 300 K. (c) Sketch of the magnetic charges and magnetic stray field which are present in the domain wall at 400 K. (d) Formation of a circular Bloch line at at 300 K.

magnetic easy plane without cost of magnetocrystalline anisotropy energy. Only stray-field energy has to be paid, which is however reduced by the segmentation [14]. The Bloch wall angle at a point of the wall where $M_y/M_S = 1$ is shown in figure 12(b) as a function of position along the z-direction. In the centre of the segments, a full out-of-plane orientation is reached. Between the segments, both the x- and y-components become zero and the z-component is plus one on the left-hand side and minus one on the right-hand side of the array as presented in figure 12(c). These orientations correspond to the initial magnetisation directions with which the simulations were started at 400 K, meaning that the domain walls contain the information concerning the initial direction of magnetisation.

For all considered temperatures, the domain wall widths for both walls, oriented parallel to the c- and a-axis, were determined according to the definition of Lilley [19]. In the case of the segmented walls, the calculation was performed at a point of maximum out-of-plane component of magnetisation. The values are summarised in table 2. One observes that with decreasing temperature the domain wall width of the wall parallel to the c-axis increases while for the other wall the trend is opposite. In both cases the wall width becomes larger with decreasing wall angle, meaning the difference of the orientation of the spins on both sides of the wall.

To find out if the domain structure described in the previous section depends on the type of pinning centre, two further types of pinning centres were analyzed. In the next two sections, the results of the simulation for pinning centres with reduced saturation magnetisation as well as for pinning centres with reduced magnetocrystalline anisotropy are summarised.

3.2.2. Pinning centre with $M_S = 0$

In the 500 times 500 matrix for each layer, the magnetisation M_S was set 1 everywhere except in the region (244|1) − (249|4) and (244|497) − (249|500), where M_S was zero, corresponding to a non-magnetic hole acting as a pinning centre.

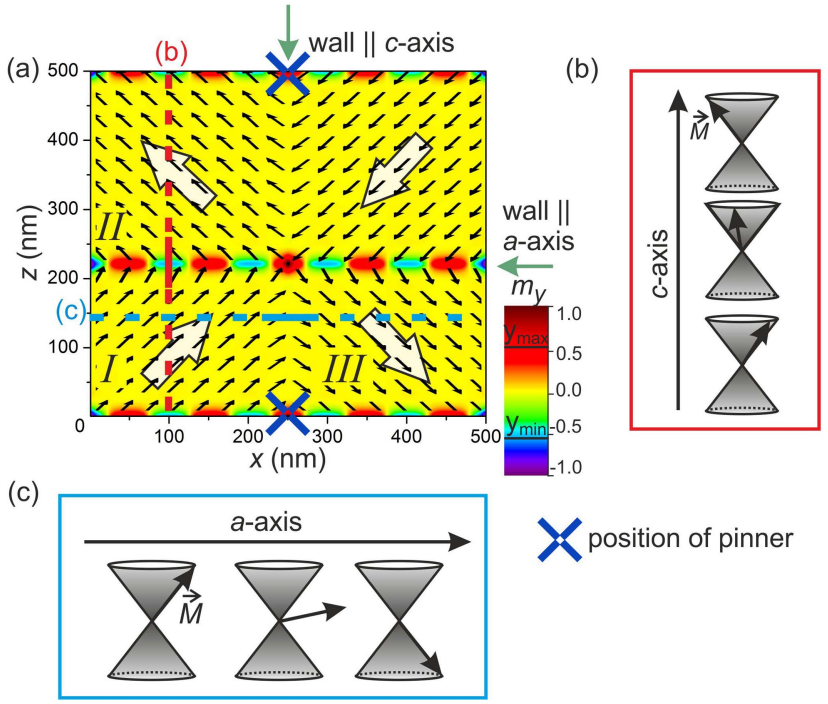

Figure 10. (a) Magnetisation projected on the *x*–*z*-plane (arrows) with underlying colour-code representing the *y*-component for 285 K (the light coloured arrows indicate the averaged direction of magnetisation within the domains), (b) orientation of the magnetic moments across the wall parallel to the *a*-axis and (c) parallel to the *c*-axis.

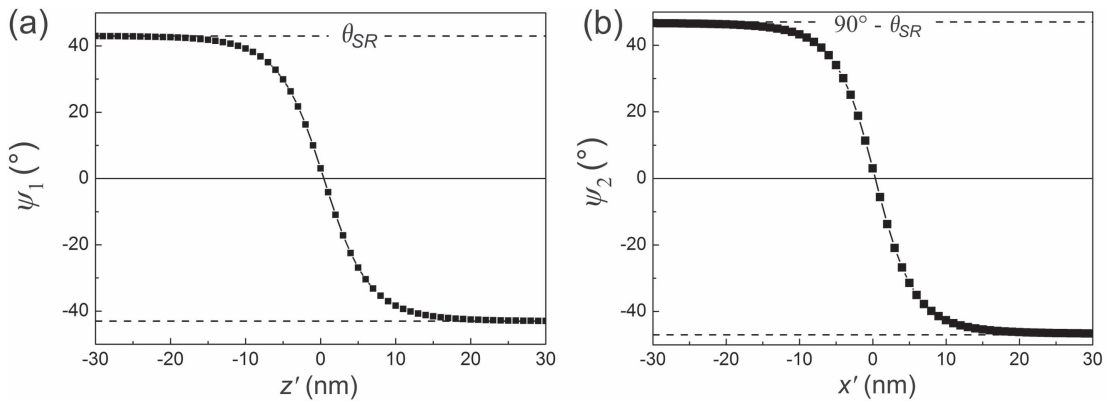

Figure 11. Orientation of the magnetic moments along the cross section of the domain wall parallel (a) to the *a*-axis and (b) to the *c*-axis at 285 K. For the definition of ψ_1 and ψ_2 see figure 5.

The simulation for 400 K leads to equivalent results as for the pinning centres with reduced exchange stiffness constant. A Bloch wall is formed which is located between the two pinning centres (figure 13(a)). Cooling down to 300 K also yields a four-domain state with circular and cross Bloch lines. But there is one difference. While in the case of the exchange pinning centres, a circular Bloch line is created at its position, in the case of a non-magnetic hole a cross Bloch line develops around the pinning centre (figure 14).

The emergence of the cross Bloch line at the position of the pinning centre can be explained by the formation of magnetic charges at the non-magnetic hole. As it is sketched in figures 13(b)–(e), at the rim of the hole magnetic charges are accumulated which lead to a tilt of the magnetic moments in *x*-direction already in the easy *c*-axis regime. As explained above for the pinning centres with reduced exchange constant, the initial tilt of the magnetisation determines the direction of rotation of the magnetic moments when the sample is cooled down in the easy-cone state.

Cooling down further to the easy-plane state results likewise in a two-domain configuration with the domains separated by a segmented Bloch wall with the same number of segments as in the case of the exchange pinning centres.

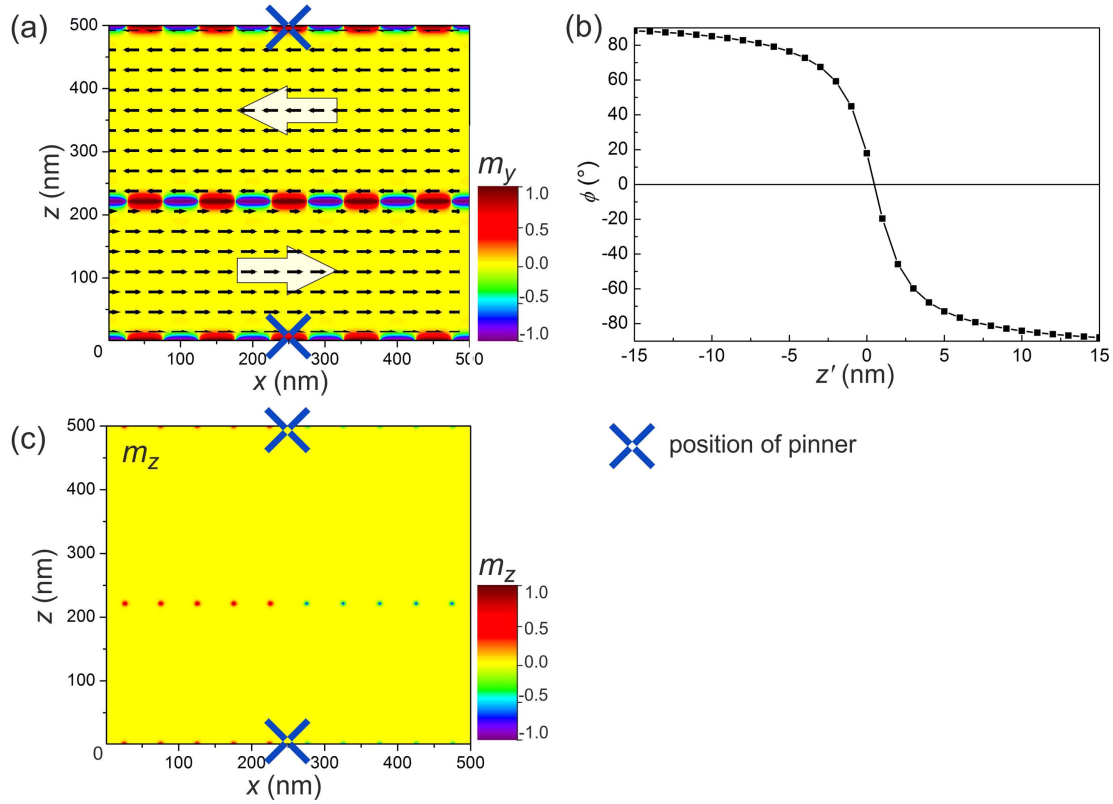

Figure 12. (a) Magnetisation configuration at 200 K (the light coloured arrows indicate the averaged direction of magnetisation within the domains), (b) Bloch wall angle at 200 K and (c) image of the *z*-component of magnetisation.

Table 2. Domain wall width derived from the simulations.

	Temperature	(K)	400	300	285	261	200
Wall ∥ *c*-axis	Wall width	(nm)	8.7	10.3	11.0	21.8	/
	Wall angle	(°)	180	142	94	38	/
Wall ∥ *a*-axis	Wall width	(nm)	/	23.2	14.1	9.5	5.6
	Wall angle	(°)	/	38	86	142	180

3.2.3. Pinning centre with $K_i' = 1/2K_i$

As a third source of pinning, reduced magnetocrystalline anisotropy constants of first and second order $K_i' = 1/2K_i$ ($i = 1, 2$) were implemented and their influence on the results of simulation was analyzed. Again, the process was started at 400 K. Equal to the other two cases, the pinning centres were placed at (248|1) − (252|2) and (248|498) − (252|500).

Like in the case of the pinning centres with reduced saturation magnetisation, the pinning centres with reduced magnetocrystalline anisotropy lead to a cross Bloch line at the position of the pinning centre (see figure 15(a)). The reduced magnetocrystalline anisotropy leads to a broadening of the domain wall, since the exchange energy becomes more important, so that the tilt between neighbouring spins becomes smaller and more magnetic moments are needed to form the domain wall. At the transition between the wider and thinner domain wall, again magnetic charges are formed (figure 15(b)), which preset the rotation of the magnetic moments when the sample is cooled down (figure 15(c)).

3.3. Comparison of simulation with measured results

Of course, real samples have a complicated microstructure consisting of grains and a dense network of pinning centres. Therefore, simulations can only represent a few special cases, e.g. one pinning centre surrounded by a homogeneous area. However, the results of the simulations reflect characteristic findings from the microscopic imaging, which was performed before on an in-plane textured $NdCo_5$ thin film by scanning electron microscopy with polarisation analysis (SEMPA) [12]. The SEMPA measurements were conducted in a temperature range between 340 and 240 K, so that the whole SRT from magnetic easy *c*-axis via easy cone to easy plane was imaged.

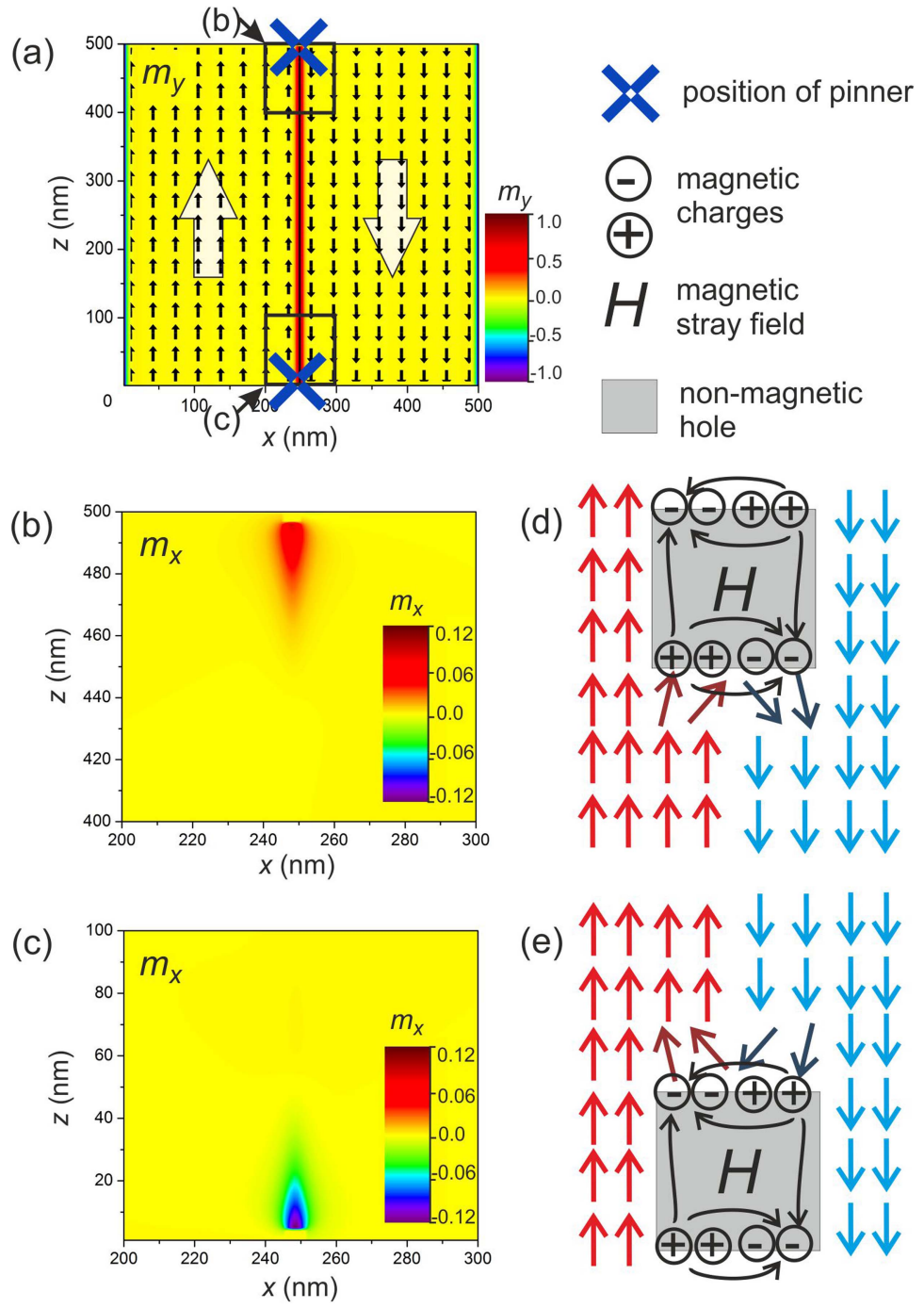

Figure 13. (a) Magnetisation configuration at 400 K for the pinning centres with $J_S = 0$ (the light coloured arrows indicate the averaged direction of magnetisation within the domains) and zoom in of the *x*-component of the magnetisation for the upper (b) and lower (c) part of the array. (d) and (e) illustrate the rotation of magnetisation near to the non-magnetic hole.

The results have shown a transition from a two-domain state in the easy *c*-axis regime with an orientation of the magnetisation parallel to the *c*-axis via a four-domain state in the magnetic easy cone regime back to a now 90° rotated two-domain state in the easy-plane regime.

Concerning the domain walls, three different orientations were identified. The domain walls with an orientation parallel to the *c*- or *a*-axis have been discussed in the simulation part above. The third type of domain wall which is found in the SEMPA images are walls with an orientation of about 45° with respect to the *c*-axis. This type of domain wall was not considered in the simulations, since the implementation of a tilted domain wall in periodic boundary conditions appeared to be quite complicated and was not realised up to now. A statistical analysis of above described domain wall orientations was performed in [20]. It has to be noticed that all present domain walls are assigned to one of the three groups, meaning that also walls with a misorientation are counted

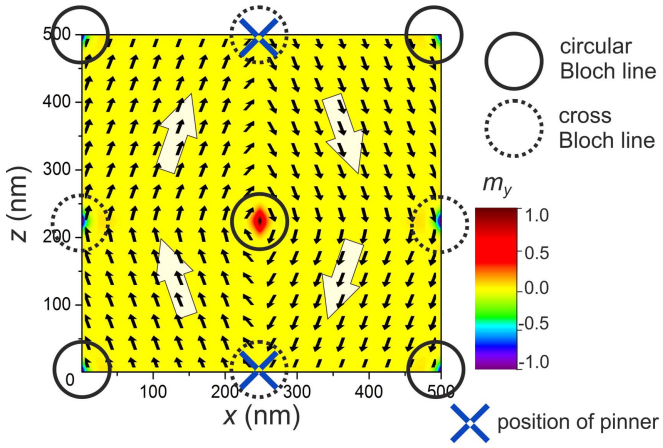

Figure 14. Magnetisation configuration at 300 K for the pinning centres with $J_S = 0$ (the light coloured arrows indicate the averaged direction of magnetisation within the domains).

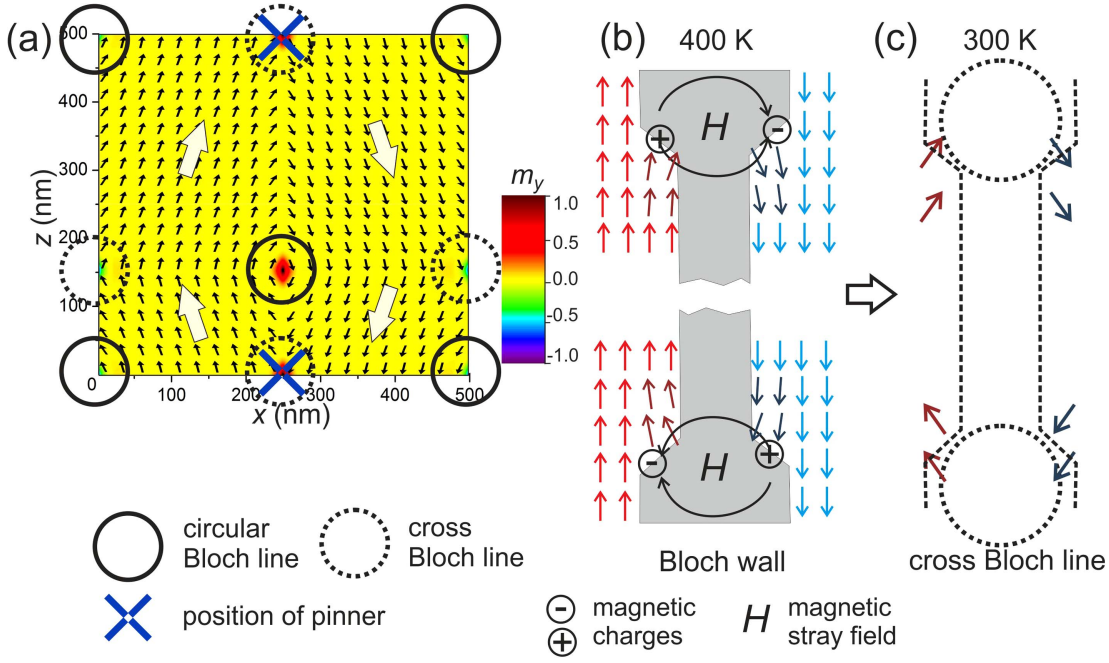

Figure 15. (a) Magnetisation configuration at 300 K for a pinning centre with reduced magnetocrystalline anisotropy constants (the light coloured arrows indicate the averaged direction of magnetisation within the domains). (b) Magnetic charges at 400 K and (c) formation of a cross Bloch line.

as '*c*-axis, *a*-axis or 45°-oriented'. Nevertheless the misalignment from the exact value can be estimated to be less than $\pm 10°$.

In the easy *c*-axis state, domain walls parallel to the *c*-axis account for 65% of all present walls, the 45° walls are less frequent (32%) and hardly any walls parallel to the *a*-axis are present [20]. In the easy-plane regime, walls parallel to the *a*-axis are dominant (82%), again followed by the 45° walls (18%) and hardly no walls parallel to the *c*-axis (1%) exist. In the easy-cone regime, all three types of domain walls are present, namely 50% of walls parallel to the *c*-axis, 30% 45° walls and 20% of walls parallel to the *a*-axis. The statistics on *a*-axis and *c*-axis oriented walls and their relative change with temperature are fully corroborated by the micromagnetic simulations, which show that along with the reorientation of magnetisation also the orientation of the domain walls changes.

Figure 16 presents a comparison of a characteristic zoomed region of the SEMPA images with the results of the simulations for the three regimes of magnetocrystalline anisotropy, i.e. easy *c*-axis, easy cone and easy plane. For this comparison, the results of the simulations display the in-plane component of magnetisation which is drawn with the same colour-code as it is used for the SEMPA images. The results are in good agreement. In the

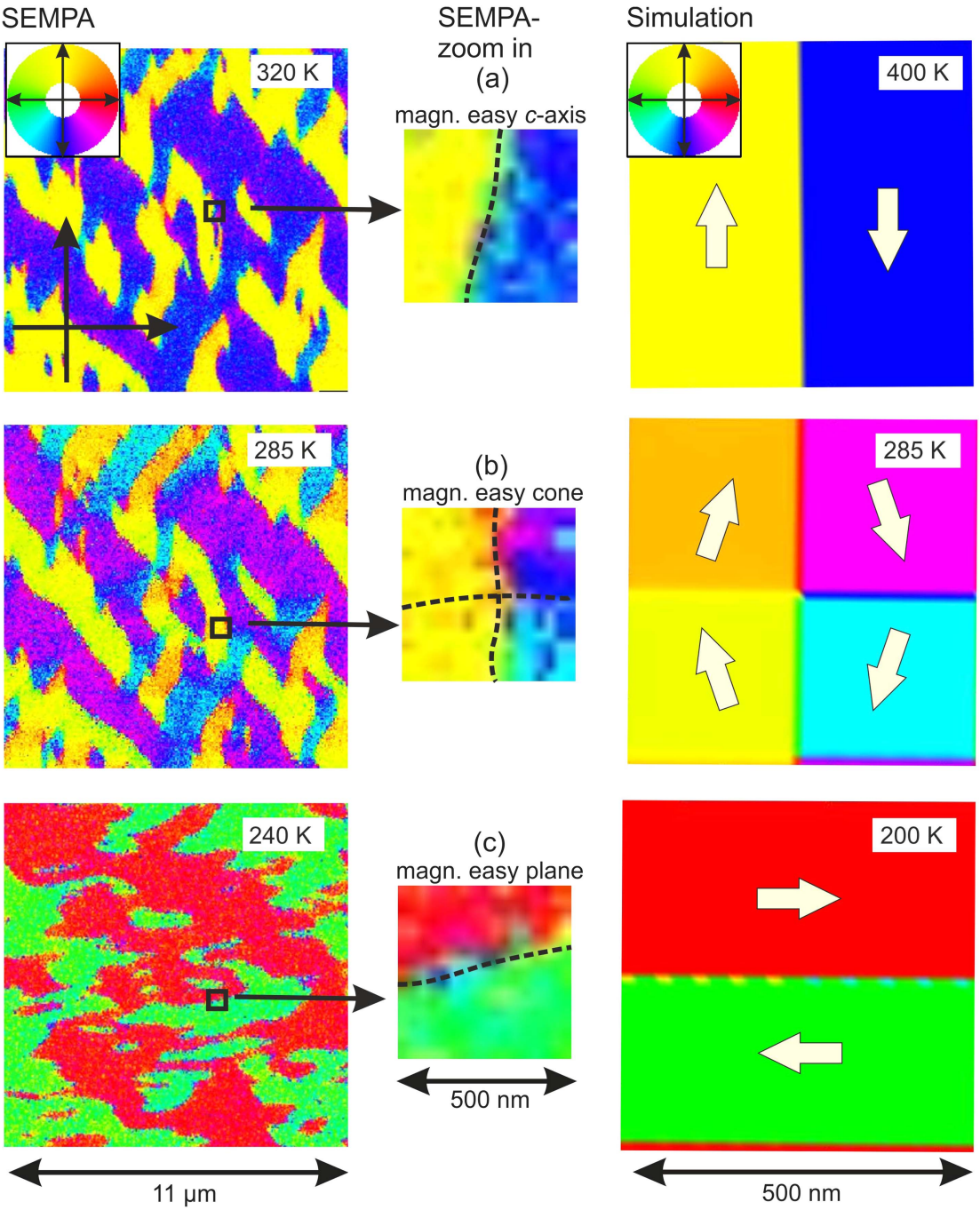

Figure 16. Comparison of SEMPA measurements [12] to the results of the simulation for (a) magnetic easy plane, (b) magnetic easy cone and (c) magnetic easy *c*-axis regime. The light coloured arrows indicate the averaged direction of magnetisation within the domains. The dashed lines in the zoomed images indicate the orientation of the domain walls. The simulations were performed with pinning centres with reduced exchange stiffness constant as discussed in section 3.2.1.

easy axis regime, the zoomed position shows a two-domain state separated by a domain wall, which is oriented almost parallel to the *c*-axis (figure 16(a)). At lower temperatures in the easy-cone state, a four-domain state evolves and an additional domain wall which is almost parallel to the *a*-axis develops (figure 16(b)). Cooling down to lowest temperatures into the easy-plane regime leads to a two-domain state with an orientation of the magnetisation and a domain wall oriented approximately parallel to the *a*-axis (figure 16(c)). The deviation of the direction of the domain walls with respect to the *a*- or *c*-axis is less than 10°.

As already mentioned above, for this comparison between the calculated and measured domain pattern we are limited to the domain walls which are oriented parallel to the *a*- or *c*-axis since the 45° domain walls have not been realised in the simulations yet.

4. Conclusions

This paper presents a micromagnetic analysis of domain processes and domain walls in $NdCo_5$ thin films. This material is especially interesting since it undergoes a spin-reorientation transition and since the magnetocrystalline anisotropy not only depends on K_1 which changes its sign with temperature but also on a large K_2 value. For those materials no analytical theory for domain walls is available, so that micromagnetic simulations are applied for the first time.

The domain pattern, the character of the domain walls and the domain wall width was investigated for the three different regimes of magnetocrystalline anisotropy.

The comparison between homogeneous systems and systems with inhomogeneities confirm the large influence of pinning centres on the domain pattern. While in undisturbed systems a two-domain state is formed when the system is cooled down into the easy-cone regime, the presence of pinning centres leads to a four-domain state in the regime of the magnetic easy cone and therefore to an improved reproduction of the measured domain pattern. Small local stray fields at the inhomogeneities are identified as driving forces for the different domain evolution.

It is shown that the character and the width of the domain wall depend on the regime of magnetocrystalline anisotropy and on the orientation of the domain wall with respect to the crystallographic *c*-axis. The wall parallel to the *c*-axis undergoes a transition from Bloch wall in the easy *c*-axis regime to a Néel wall in the easy-cone regime. It disappears in the easy-plane state. Walls parallel to the *a*-axis are not present in the easy-axis state. A Néel wall parallel to the *a*-axis develops in the presence of unavoidable defects/pinning sites when the sample is cooled down into the easy-cone regime. By lowering the temperature, the character changes to a mixed wall type (both Néel and Bloch contributions) and finally results in a segmented Bloch wall in the easy-plane regime, where the segmentation leads to a reduction of stray-field energy.

The simulations revealed interesting domain wall features, which wait for experimental verification. High resolution magnetic imaging will be necessary to observe the domain wall structure.

Acknowledgments

Part of this work was funded by the German National Academic Foundation. The SEMPA study was carried out with financial support from DFG within SFB668.

References

[1] Nikitin S A, Skokov K P, Koshkid'ko Y S, Pastushenkov Y G and Ivanova T I 2010 *Phys. Rev. Lett.* **105** 137205
[2] Teixeira B M S, Timopheev A A, Schmidt R, Soares M R, Seifert M, Neu V and Sobolev N A 2016 *J. Phys. D: Appl. Phys.* **49** 315002
[3] Bartholin H, van Laar B, Lemaire R and Schweizer J 1966 *J. Phys. Chem. Solids* **27** 1287
[4] Klein H P, Menth A and Perkins R S 1975 *Physica* B **80** 153
[5] Bartashevich M I, Goto T, Yamaguchi T M, Yamamoto I and Radwanski R J 1993 *Solid State Commun.* **87** 1093–5
[6] Ohkoshi M, Kobayashi H, Katayama T, Hirano M and Tsushima T 1976 *AIP Conf. Proc.* **29** 616
[7] Alameda J M, Givord D, Lemaire R and Lu Q 1981 *J. Appl. Phys.* **52** 2079–81
[8] Adreev A V, Deryagin A V and Zadvorkin S M 1982 *Phys. Status Solidi* a **70** K113
[9] Patterson C, Givord D, Voiron J and Palmer S B 1986 *J. Magn. Magn. Mater.* **54** 891–2
[10] Seifert M, Schultz L and Neu V 2009 *J. Appl. Phys.* **106** 073915
[11] Seifert M, Schultz L and Neu V 2010 *J. Appl. Phys.* **107** 09A711
[12] Seifert M, Schultz L, Schäfer R, Neu V, Hankemeier S, Rössler S, Frömter R and Oepen H P 2013 *New J. Phys.* **15** 013019
[13] Frömter R, Hankemeier S, Oepen H P and Kirschner J 2011 *Rev. Sci. Instrum.* **82** 033704
[14] Hubert A and Schäfer R 1998 *Magnetic Domains* (Berlin: Springer)
[15] Träuble H, Boser O and Kronmüller H 1965 *Phys. Status Solidi* **10** 283
[16] Benaissa M, Krishnan K M, Fullerton E E and Jiang J S 1998 *IEEE Trans. Magn.* **34** 1204
[17] Berkov D V and Gorn N L MicroMagus—package for micromagnetic simulations www.micromagus.de
[18] Guo Z J, Jiang J S, You C Y, Vlasko-Vlasov V K and Welp U 2003 *J. Appl. Phys.* **93** 8122
[19] Lilley B A 1950 *Phil. Mag.* **41** 792–813
[20] Hankemeier S 2010 The magnetic fine structure of thin-film elements *PhD Thesis* Universität Hamburg ,Germany